Volume 26
Number 8
28 February 2024
Pages 6461–7242

PCCP

Physical Chemistry Chemical Physics

rsc.li/pccp

25 YEARS ANNIVERSARY

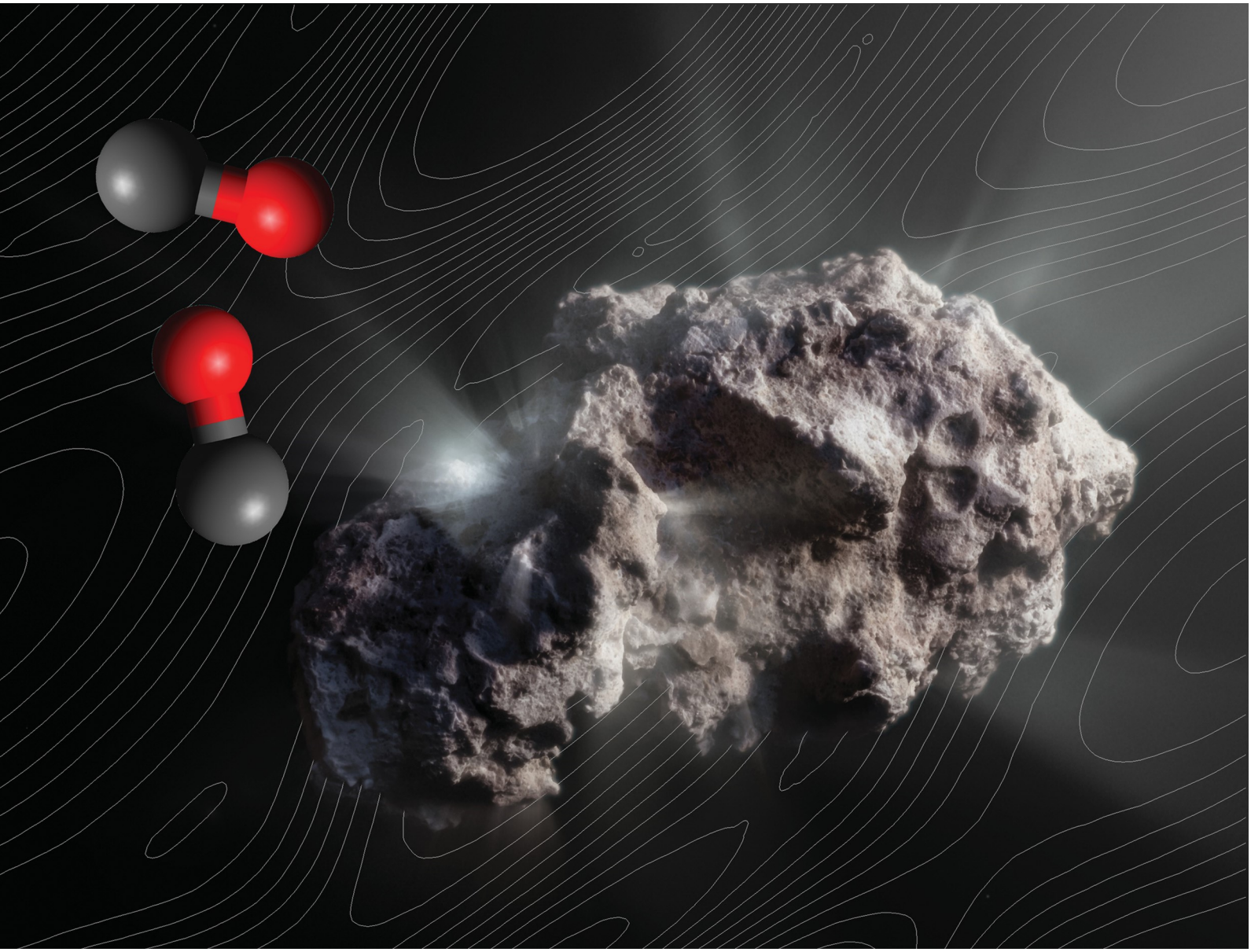

ISSN 1463-9076

ROYAL SOCIETY OF CHEMISTRY

PAPER

Dmitri Babikov *et al.*

Mixed quantum/classical calculations of rotationally inelastic scattering in the CO + CO system: a comparison with fully quantum results

PCCP Owner Societies

PCCP

PAPER

Cite this: *Phys. Chem. Chem. Phys.*, 2024, **26**, 6627

Mixed quantum/classical calculations of rotationally inelastic scattering in the CO + CO system: a comparison with fully quantum results†

Dulat Bostan, [a] Bikramaditya Mandal, [a] Carolin Joy, [a] Michał Żółtowski, [b] François Lique, [b] Jérôme Loreau, [c] Ernesto Quintas-Sánchez, [d] Adrian Batista-Planas, [d] Richard Dawes [d] and Dmitri Babikov *[a]

An updated version of the CO + CO potential energy surface from [R. Dawes, X. G. Wang and T. Carrington, *J. Phys. Chem. A* 2013, **117**, 7612] is presented, that incorporates an improved treatment of the asymptotic behavior. It is found that this new surface is only slightly different from the other popular PES available for this system in the literature [G. W. M. Vissers, P. E. S. Wormer and A. Van Der Avoird, *Phys. Chem. Chem. Phys.* 2003, **5**, 4767]. The differences are quantified by expanding both surfaces over a set of analytic functions and comparing the behavior of expansion coefficients along the molecule–molecule distance *R*. It is shown that all expansion coefficients behave similarly, except in the very high energy range at small R where the PES is repulsive. That difference has no effect on low collision-energy dynamics, which is explored *via* inelastic scattering calculations carried out using the MQCT program which implements the mixed quantum/classical theory for molecular energy exchange processes. The validity of MQCT predictions of state-to-state transition cross sections for CO + CO is also tested by comparison against full-quantum coupled-states calculations. In all cases MQCT gives reliable results, except at very low collision energy where the full-quantum calculations predict strong oscillations of state-to-state transition cross sections due to resonances. For strong transitions with large cross sections, the results of MQCT are reliable, especially at higher collision energy. For weaker transitions, and lower collision energies, the cross sections predicted by MQCT may be up to a factor of 2–3 different from those obtained by full-quantum calculations.

Received 5th November 2023,
Accepted 14th December 2023

DOI: 10.1039/d3cp05369e

rsc.li/pccp

I. Introduction

Comets carry the most pristine material in the solar system, deposited during the epoch of its formation.[1] They hold a record of the composition of the proto-solar accretion disc and can offer unique insight into the photochemistry and thermochemistry of planet and star formation of our solar system.[2] The molecular composition of cometary comae typically correlates with their distance from the sun and includes several volatile ices, such as H_2O, CO_2, CH_4, CO and NH_3. For example, the comets of the Kuiper Belt (those closest to the sun with a period of orbit on the order of a few years) contain higher amounts of H_2O and CO_2, while the comets of the Oort Cloud (those that come from the furthest parts of the solar system, with colder temperature, and have a period of orbit on the order of 10 000 years) exhibit elevated abundances of CO and NH_3.[3] A new class of objects, called the interstellar comets such as 2I/Borisov,[4–7] exhibit an anomalously large abundance of CO,[8,9] a factor of 10 brighter than typical Kuiper Belt comets, suggesting that they originated in the coldest environment. The eccentricity of their orbits indicates that they came from outside the solar system, bringing information about the diversity of the proto-planetary discs in the galaxy.[1,10] Note that CO is important as a precursor for oxygen-bearing complex organic molecules in the universe.

As comets approach the sun, their material sublimes and forms a cometary coma – a transient atmosphere that can be observed from Earth or from satellites and analyzed using the tools of spectroscopy. Energy transfer in the outermost part of the expanding gas is controlled by fluorescence, while the inner (most dense) part of the coma is controlled by molecule–molecule

[a] *Chemistry Department, Marquette University, Milwaukee, Wisconsin 53201-1881, USA. E-mail: dmitri.babikov@mu.edu*
[b] *Univ Rennes, CNRS, IPR (Institut de Physique de Rennes)-UMR 6251, F-35000 Rennes, France*
[c] *KU Leuven, Department of Chemistry, B-3001 Leuven, Belgium*
[d] *Department of Chemistry, Missouri University of Science and Technology, Rolla, Missouri 65409, USA*

† Electronic supplementary information (ESI) available. See DOI: https://doi.org/10.1039/d3cp05369e

collisions, such as CO + CO. In the intermediate part, called mid-coma, the two processes compete, and the populations of molecular states deviate from local thermodynamic equilibrium.[11] For this reason, the interpretation of cometary observations requires computer modeling of the radiation transfer, using codes such as RADEX[12] or LIME.[13] These simulations, in turn, require as input, the rate coefficients for collisional energy transfer between the chemical species of the coma. In recent years, physical chemists generated several databases of rotational state-to-state transition rate coefficients for typical cometary molecules abundant in the comets, such as H_2O + CO,[14] HCN + H_2O,[15] H_2O + H_2O,[16,17] and CO + CO.[18–20]

The focus of this paper is on CO + CO collisional energy transfer, important for the modeling of cometary atmosphere of comets observed at large heliocentric distances. Several potential energy surfaces exist for the CO + CO interaction. One of the popular surfaces, built about 20 years ago by Vissers *et al.*[21] for their studies of state-to-state transition cross sections in molecular beam experiments,[22] was recently used in a series of papers[18,19] to generate a set of thermal rate coefficients for state-to-state transitions between the rotational states of CO up to j = 10 at the temperatures up to T = 150 K. Another surface was built by Dawes *et al.* for the prediction of spectra of weakly bound CO···CO van der Waals complex[23] (vdW) and was also used to compute rate coefficients for several individual transitions.[20] Finally, a 6D surface that includes the vibrational degrees of freedom of both collision partners was built by Chen *et al.*[24] to study the vibrational relaxation of CO relevant to supersonic CO lasers[25] using a classical trajectories method. Since in this paper the emphasis is on rotational transitions, we focus on the two former PESs, those of Vissers *et al.*[21] and Dawes *et al.*[23]

The original 2013 PES of Dawes *et al.*, motivated by a spectroscopic study of the CO···CO complex, did not include an accurate description of the asymptotic long-range interaction, which is critical for the description of CO + CO scattering in low-temperature environments. Therefore, one goal of this paper is to report an updated version of that PES, which now includes an accurate treatment of the asymptotic range that connects seamlessly to the short-range interaction. This new PES is compared to the PES of Vissers *et al.*[21] through analysis of the PES expansion radial coefficients and by conducting new scattering calculations on different PESs.

The main goal of this paper is to test a promising approach for inelastic scattering calculations, the so-called mixed quantum/classical theory (MQCT).[26–28] This method combines classical mechanics for the description of translational motion of two collision partners with a quantum mechanical description of their rotational motion,[29–31] which permits simplifying the model and accelerating the calculations of scattering cross sections, while keeping the most important physics associated with inelastic transitions between the quantized states of collision partners. Here, new MQCT calculations are carried out to compute cross sections for state-to-state transitions between the rotational states of two colliding CO molecules and the results are compared with previously published results of the full-quantum calculations.[18]

II. *Ab initio* method and pes fitting

As depicted in Fig. 1, the coordinates used to represent the vdW interaction between the two closed–shell CO monomers are the Jacobi coordinates: R, θ_1, θ_2, and φ. In the figure, $\vec{R}$ is the vector between the centers of mass of the two fragments, and $\vec{r}_1$ and $\vec{r}_2$ are vectors aligned with each molecule. The coordinate R is the length of vector $\vec{R}$, while coordinates θ_1 and θ_2 represent (respectively) the angles between $\vec{R}$ and the vectors $\vec{r}_1$ and $\vec{r}_2$. The fourth coordinate is the dihedral (out of plane) torsional angle, labeled φ, which is the angle between the vectors $\vec{R} \times \vec{r}_1$ and $\vec{R} \times \vec{r}_2$ Notice that for $\theta_1 = \theta_2 = 0^\circ$ the molecules are aligned end-to-end, with the carbon atom in the first molecule pointing to the oxygen atom of the second molecule.

As we have done in the past for other vdW dimers of linear fragments,[32–37] the PES's analytical representation was constructed using an automated interpolating moving least squares (IMLS) methodology, freely available as a software package under the name AUTOSURF.[38] As usual,[39,40] a local fit was expanded about each data point, and the final potential is obtained as the normalized weighted sum of the local fits. The fitting basis and most other aspects of the IMLS procedure were the same as for other previous systems and have been described in detail elsewhere.[38,40,41] All *ab initio* calculations were performed using the Molpro electronic structure code package.[42]

For construction of the PES, both monomers were held rigid. The bond distance for CO was fixed at r_{CO} = 1.128206 Å, the vibrationally-averaged bond distance for the ground rovibrational state of CO, consistent with its rotational constant of B_0 = 1.9317 cm^{-1}. Masses of 15.9949146221 and 12 μ were used for ^{16}O and ^{12}C, respectively. The 2013 study by Dawes *et al.* generated at least nine different PESs, exploring the effects of basis-set completeness, testing various basis extrapolation schemes, as well as the effect of including core-electrons in the correlation treatment. The new PES reported here with an improved treatment of the long range, was also computed using explicitly-correlated coupled-cluster theory[43] (CCSD(T)-F12b), with details chosen to closely match what was determined to be the most accurate of the 2013 PESs.

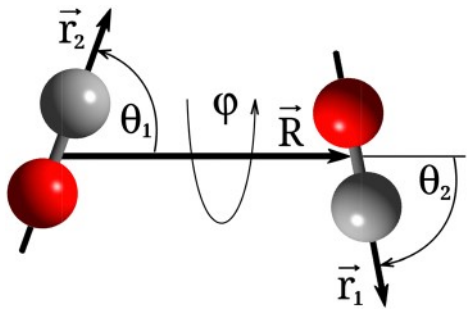

Fig. 1 Coordinates used to describe the CO dimer interaction.

For consistency with the added data in the long range, the entire dataset was recomputed using Molpro2019. Here the complete basis set limit was estimated by extrapolating total energies at the CCSD(T)-F12b/CVTZ-F12 and CCSD(T)-F12b/CVQZ-F12 levels, using a two-basis formula suggested by Schwenke [eqn (8) in ref. 44] with a coefficient of precisely 1.4. All electrons were included in the correlation treatment and geminal beta coefficients of 1.4 and 1.5 were specified for the CVTZ-F12 and CVQZ-F12 bases respectively, in the F12b calculations. This level of electronic structure theory is expected to provide a more accurate description of interaction potential, compared to the method employed by Vissers *et al.* for the older PES. Also, this basis set is larger compared to the basis set employed by Chen *et al.*, which places the present PES at the top of the list for the scattering studies of rigid CO molecules. The PES by Chen *et al.*, although based on slightly less accurate *ab initio* points, is a full dimensional PES that allows for a wider range of applications.

The shortest intermonomer center-of-mass distance considered is R = 2.6 Å, with the additional restriction of a maximum repulsive energy of 6 kcal mol^{-1} ($\sim$2100 cm^{-1}) above the separated monomers' asymptote. The *ab initio* data coverage in the fitted PES extends to R = 15 Å, which is extended by an analytic form, informed by additional data at the same level extending to R = 30 Å, with the zero of energy set at infinite separation between the monomers. The long-range form includes electrostatics up to 7th order, beginning with the 3rd order dipole–dipole interaction, as well as induction and dispersion terms, which both start at 6th order in this uncharged system, and are also truncated at 7th order. This expression is both physically correct and sufficiently flexible to fit the data computed in the long range essentially exactly (RMSE $<$ 0.003 cm^{-1}). The exchange symmetry of the PES expected for identical monomers is respected precisely.

The global fit switches smoothly from interpolated *ab initio* data in the close interaction region, to the analytic long range *via* a hyperbolic tangent function centered at R = 7.5 Å, which also gives a smooth gradient and a continuous Hessian of the PES with respect to R. We also checked and confirmed that in this range of R a smooth behavior is obtained for the coefficients $v(R)$ of PES expansion (see below), for the elements of state-to-state transition matrix, and for their gradients and Hessians. This is presented by Fig. S1 of ESI.†

For the high-level PES, the global estimated root-mean-squared fitting error is 0.82 cm^{-1}, and the total number of automatically generated symmetry-unique points needed to reach that target was 3164 (the final estimated error is 0.04 cm^{-1} for energies below the asymptote). To guide the placement of high-level data, avoiding placing expensive high-level data in energetically inaccessible regions, a lower-level guide surface was constructed using 2568 symmetry-unique points, distributed using a Sobol sequence[45] biased to sample the short-range region more densely. This was done at the CCSD(T)-F12b/VDZ-F12 level of theory.

The analytical representation of the PES is available from the authors upon request.

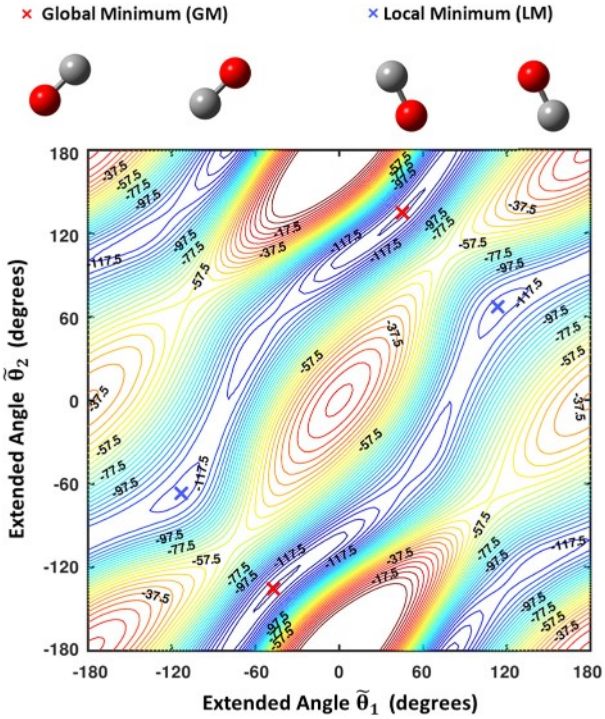

Fig. 2 R-optimized contour plot of the PES as a function of the extended angles $\tilde{\theta}_1$ and $\tilde{\theta}_2$ for planar configurations. For each pair of angles, the energy (given in cm^{-1}) is optimized with respect to the center-of-mass distance R. See the text for details.

Fig. 2 shows a 2D representation of the PES (denoted R-optimized) as a function of the extended angles $\tilde{\theta}_1$ and $\tilde{\theta}_2$ for planar configurations ($\varphi = 0^\circ$ and $\varphi = 180^\circ$). The positions of the minima and their corresponding molecular configurations are also highlighted in the figure. Each of the extended-angle coordinates $\tilde{\theta}_1$ and $\tilde{\theta}_2$ spans a full 360°, varying in the range from −180° to +180°, which gives a continuous description of motions on the global PES as described in detail elsewhere.[2,3] A consequence of this, mentioned below, is that each minimum (or other feature) appears twice in the plot. For planar geometries ($\varphi = 0^\circ$ for quadrants II and IV, and $\varphi = 180^\circ$ for quadrants I and III), the plot describes the complete ranges of $\tilde{\theta}_1$ and $\tilde{\theta}_2$, relaxing the intermonomer distance coordinate R for each pair of angles. This type of plot provides useful insight into the behavior of the system, since for many systems, those (such as this one) without non-planar minima, the plot will include all isomers and planar isomerization paths between them, making it easy to visualize motions during which φ changes from 0° to 180°. There are two minima in the PES, each appearing twice in the extended angles plot. Both minima configurations correspond to skew-parallel structures. The global minimum (GM), with a well depth of 134.0 cm^{-1}, has the carbon atoms closer; while the local minimum (LM), with a well depth of 118.8 cm^{-1}, has the oxygen atoms closer. A disrotatory (or geared) motion moves the system along a nearly barrierless low-energy-path connecting the minima (*cf.* Fig. 2). As explored previously,[2,3] low lying rovibrational states tend to delocalize significantly along the geared motion channel. Table 1 provides geometric

Table 1 Geometric parameters and energies (Angstroms, degrees, and wavenumbers) for the global (GM) and local minima (LM)

	Present PES		Vissers *et al.*[21]	
	GM	LM	GM	LM
R	4.328	3.620	4.339	3.678
θ_1	45.4	113.7	45.8	120.4
θ_2	134.6	66.3	134.2	59.6
φ	180.0	180.0	180.0	180.0
V	134.0	118.8	135.5	124.2

parameters of the two minima, comparing also with those from the PES by Vissers *et al.* The values are generally similar, differing most significantly for the angles of the LM. This difference was discussed previously in the 2013 paper by Dawes *et al.* noting that the PES by Vissers *et al.* is empirically adjusted and has more significant fitting error and even a spurious minimum, so the present PES should be more reliable in this respect. Nevertheless, perhaps since the CO–CO interaction energy is quite flat along the geared motion channel, both PESs yield reasonable rovibrational levels.

Fig. 3 plots ten radial cuts through the PES, each corresponding to different orientational poses of the monomers. The plot compares the fitted PES with independently computed test data, which in addition to the fitting error statistics mentioned earlier, helps confirm good fitting behavior. The leading terms governing the shape of the long-range region of the PES come from the dipole–dipole, dipole–quadrupole, and quadrupole–quadrupole electrostatic interactions, which have R^{-3}, R^{-4}, and R^{-5} radial dependencies, respectively.

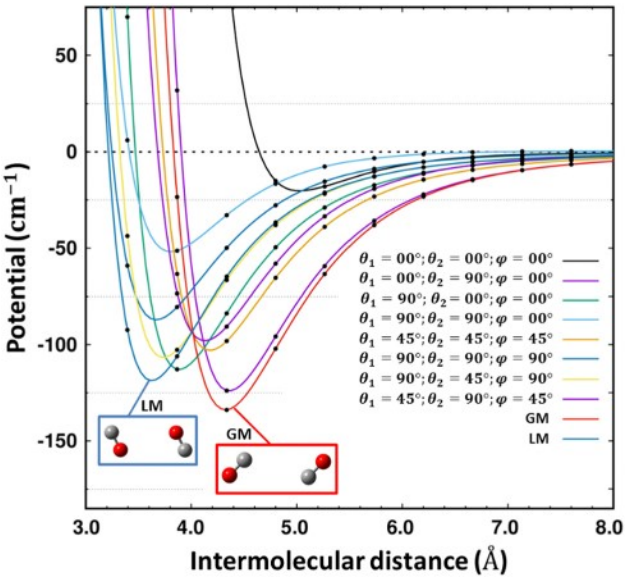

Fig. 3 Radial cuts through the PES are plotted for various orientational poses of the two monomers including those that pass through the two minima (geometric parameters of the minima are given in Table 1). The lines represent the fitted PES, while the points are *ab initio* data not included in the fitting set, which helps verify the fitting accuracy. The variation in the cuts illustrates the anisotropy of the PES and highlights the substantial difference in the radial coordinate for the two minima.

III. Scattering calculations

Calculations of state-to-state transition cross sections were carried out within the framework of the mixed quantum/classical theory, using MQCT program.[27] In order to make comparison with full-quantum calculations straightforward, we treated the colliding CO molecules as distinguishable and used an approximate coupled-states version of the theory, CS-MQCT, since a similar approach was employed by ref. 18. In CS-MQCT the Coriolis couplings are neglected, and all state-to-state transitions are driven only by potential couplings. The details of the CS-MQCT approximation were presented in ref. 46. The derivation of MQCT theory for diatom + diatom systems can be found in ref. 47 and 48.

A large basis set of rotational eigenstates was employed for both collision partners, up to $(j_1,j_2) = (15,15)$, which has the energy of $\sim$922 cm^{-1}, still well below that of the lowest quantum of vibrational energy in CO. The range of molecule–molecule distances $2.65 \le R \le 26.5$ Å (or $5 \le R \le 50$ Bohr) was covered by a grid of 76 points with logarithmic spacings (denser at short range and sparser in the asymptotic region). The angular dependence of the PES was described *via* expansion over a basis set of analytic functions, symmetrized to represent CO + CO:[27]

$$\tau_{\lambda_1\lambda_2\lambda}(\theta_1,\pi-\varphi,\theta_2) = \sum_{\eta=-\min(\lambda_1,\lambda_2)}^{+\min(\lambda_1,\lambda_2)} C^{\lambda,0}_{\lambda_1,\eta,\lambda_2,-\eta} Y^{\lambda_1}_{+\eta}(\theta_1,0)\, Y^{\lambda_2}_{-\eta}(\theta_2,\pi-\varphi) + C^{\lambda,0}_{\lambda_2,\eta,\lambda_1,-\eta} Y^{\lambda_2}_{+\eta}(\theta_1,0)\, Y^{\lambda_1}_{-\eta}(\theta_2,\pi-\varphi) \quad (1)$$

The expansion was truncated to retain 56 potential terms up to $\lambda_1 = \lambda_2 = 5$. Integration over θ_1 and θ_2 was done using Gauss–Legendre quadrature with 20 points in each degree of freedom, while for integration in φ an equidistant grid of 40 points was used. These convergence parameters for the MQCT calculations are either identical or similar to those of full-quantum calculations of ref. 18 and 19.

The maximum impact parameter for MQCT calculations was b_{max} = 10.6 Å (or 20 Bohr), which corresponds to the orbital angular momentum quantum number ℓ_{max} = 98 for the lowest collision energy (100 cm^{-1}) and ℓ_{max} = 335 for the highest collision energy (1200 cm^{-1}) considered here. The dependence of partial cross sections on ℓ at collision energy 1200 cm^{-1} is presented in Fig. 4 for various state-to-state transitions originating from the ground state $(j_1,j_2) = (0,0)$. One clearly sees two groups of processes. One group contains many weaker transitions, characterized by smaller partial cross sections (on the order of 0.05 Å^2 per ℓ, see Fig. 4) and a shorter-range interaction. For these processes $\ell_{max} \sim 190$ is sufficient, since at higher values of ℓ the contributions of the partial cross sections are vanishingly small. The other group includes only four transitions: $(j_1,j_2) = (0,0) \rightarrow (0,1)$, (1,1), (0,2) and (2,2). These processes are more intense (on the order of 0.2 Å^2 per ℓ) and remain significant through much higher values of ℓ. Specifically, $\ell_{max} \sim 250$ is needed for the excitation of $(j_1,j_2) = (0,1)$

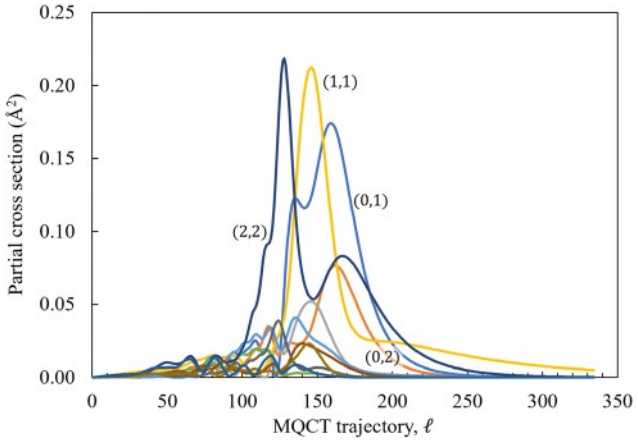

Fig. 4 Partial cross sections for excitation of various states in CO + CO collision at 1200 cm^{-1}. The initial state is (0,0). Final states (j_1,j_2) are indicated for the 4 most intense transitions. The PES of Vissers *et al.* was used for these tests.

and (0,2), $\ell_{max} \sim 300$ for the excitation of (2,2), and $\ell_{max} \sim 350$ for the excitation of (1,1). Such long-range behavior is the consequence of electrostatic interactions, beginning at dipole–dipole, in the CO + CO system.

MQCT calculations were done for three different initial states of CO + CO system which includes both molecules in the ground rotational state: $(j_1,j_2) = (0,0)$, both molecules placed in a highly excited state: $(j_1,j_2) = (8,8)$, and an intermediate mixed case: $(j_1,j_2) = (0,8)$. For the initial state (0,0) we propagated MQCT trajectories with all values of orbital angular momentum ℓ from 0 to ℓ_{max}, while for the other two cases we did Monte–Carlo sampling of the initial conditions for which the values of ℓ are sampled randomly between 0 and ℓ_{max} (simultaneously with sampling of j_{12} between $|j_1-j_2|$ and j_1+j_2 and the quantum number m_{12} in the range from 0 to j_{12}). In these cases, we found that a sample of 450 MQCT trajectories gives cross sections converged to within 1% percent.

As stated above, our rotational basis set includes all levels up to $j_{max} = 15$ for each CO molecule, which yields 256 channels of CO + CO and 65 536 states with different values of quantum numbers j_{12} and m_{12}. The number of state-to-state transitions in the original matrix was ~64.5 million. To speed up the calculations we neglected transitions between the weakly bound states, using a cutoff value of 0.1 cm^{-1} for the potential matrix elements, applied at the CO–CO distance near $R = 3.8$ and 4.2 Å. This truncation retains ~15.3 million matrix elements responsible for the most important state-to-state transitions. The error introduced by truncation is estimated to be less than 1% of the cross-section magnitudes.

IV. Results and discussion

In Fig. 5 we present a comparison of radial expansion coefficients $v_{\lambda_1\lambda_2\lambda}(R)$ that we obtained for the two potential energy surfaces of CO + CO: that of Vissers *et al.*[21] and the newly updated PES developed here. The upper frame contains radial

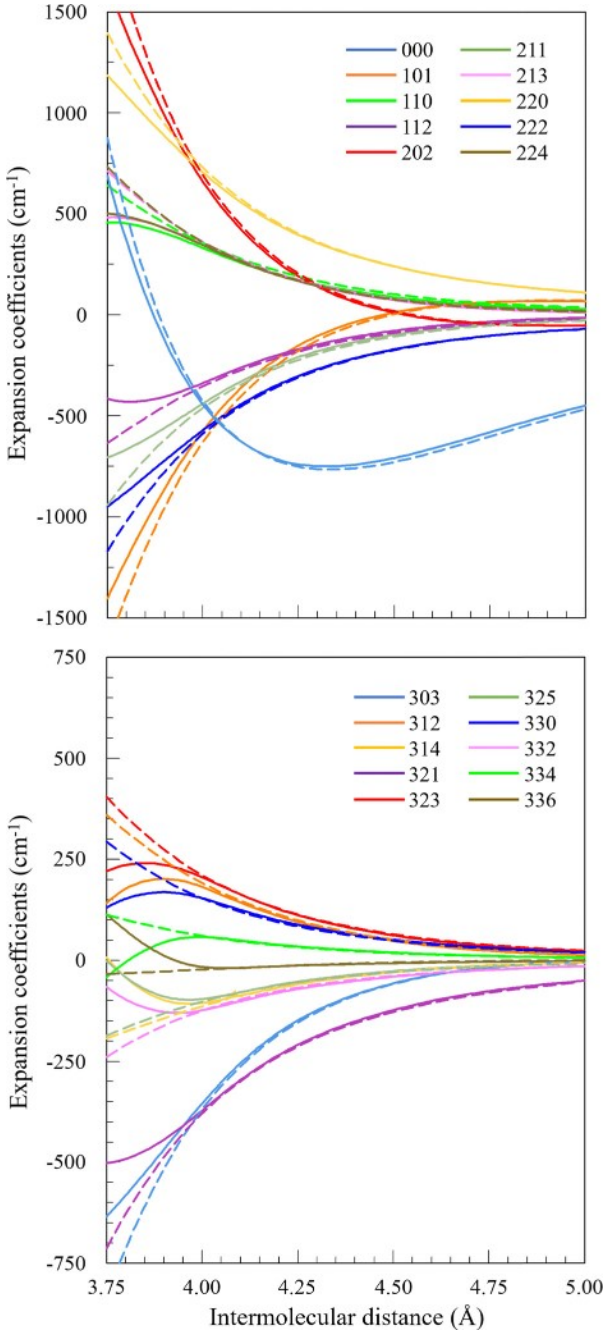

Fig. 5 Radial dependence of 20 expansion coefficients $v_{\lambda_1\lambda_2\lambda}(R)$ for two CO + CO PESs in the interaction region: This work (solid line) and Vissers *et al.* (dashed line). Colors correspond to different sets of $\lambda_1\lambda_2\lambda$, as indicated.

dependencies of the 10 largest expansion terms, including the isotropic interaction term $(\lambda_1\lambda_2\lambda) = (000)$ responsible for elastic scattering. The lower frame of Fig. 5 contains the next 10 expansion terms up to $(\lambda_1\lambda_2\lambda) = (336)$. From these figures it is seen that although the two PESs are overall similar in the range of attractive interaction, $R > 4$ Å, there are some noticeable differences in the expansion coefficients. Namely, the isotropic term (000) is deeper for the PES of Vissers *et al.* by about

20 cm^{-1}. Also, near the minimum at R = 4.3 Å, anisotropic terms (101), (110), (112), (211) and (202) differ by about 19, 17, 12, 12 and 10.5 cm^{-1}, respectively. These differences in the PESs have a significant impact on detailed comparisons of the stacks of rovibrational levels noted in the previous 2013 spectroscopic study.[23] Larger differences between the two sets of expansion coefficients are seen in the range of repulsive interaction, $R < 4$ Å, which is attributed to a truncation of the present PES at high energy. These differences are expected to have only minor effects on inelastic state to state transitions at low energies.

Fig. 6 illustrates the behavior of radial expansion coefficients $v_{\lambda_1\lambda_2\lambda}(R)$ in the asymptotic range $R > 10$ Å, for the two PESs. Here the absolute value is plotted, $|v_{\lambda_1\lambda_2\lambda}(R)|$ and a log scale is used to better appreciate the weaker long-range interactions. This figure illustrates that the value of the isotropic term of the PES expansion $(\lambda_1\lambda_2\lambda) = (000)$ drops quickly and by $R \sim 18.5$ Å becomes smaller than several anisotropic terms: $(\lambda_1\lambda_2\lambda) = (110)$, (112), (211) and (220). The largest differences between the two PESs in Fig. 6 are found in the dipole–dipole interaction terms (110) and (112) that dominate the long-range behavior. For these terms, the differences on the order of 20% are observed through the entire range 10 Å $< R <$ 25 Å. On the other hand, the expansion terms (220) and (222), responsible for quadrupole–quadrupole interaction, demonstrate small differences between the two PESs near the R = 10 Å, but at larger distances these differences also become larger, up to 66% and 111%, respectively (although their absolute values become very small at this point, around 0.015 and 0.012 cm^{-1}, respectively).

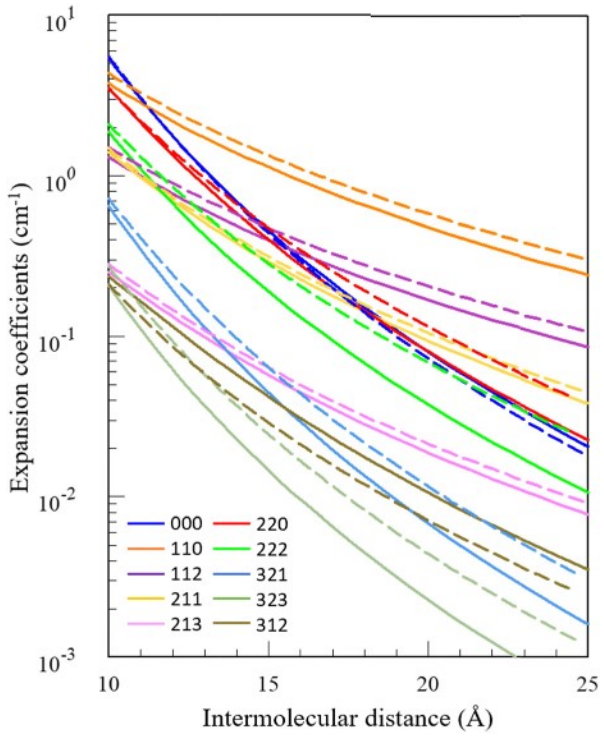

Fig. 6 Same as Fig. 5, but in the asymptotic long-range region of CO + CO for 10 selected expansion terms of the two PESs. The vertical scale gives absolute value of expansion coefficients $v_{\lambda_1\lambda_2\lambda}(R)$ in log scale.

Further comparison of the two PESs was conducted by running MQCT calculations of inelastic state-to-state transition cross sections using each surface. The results are presented in Fig. 7 for 135 individual state-to-state transitions at three collision energies. These transitions originate in the ground rotational state $(j_1,j_2) = (0,0)$ of the CO + CO system and excite either one, or both CO molecules into the combination states, up to $(j_1,j_2) = (15,15)$ with maximum total rotational energy of $\sim$922 cm^{-1}. From Fig. 7 one can see that for stronger dipole-driven transitions with the largest cross sections (on the order of 1 Å^2 and above) the two PESs produce very similar results. For weaker processes with smaller cross sections (down to 10^{-2} Å^2) the differences obtained from the two PESs do not exceed a factor of 2, which is considered an upper bound for an acceptable range of accuracy in astrophysical modeling. Moreover, the majority of data points in Fig. 7 are spread symmetrically about the diagonal line, which means that some transitions have smaller cross sections, while others have larger cross sections, without any systematic difference between the two PESs. Only at the lowest collision energy considered here (200 cm^{-1}) and for the weakest transitions (cross sections smaller than 10^{-2} Å^2) do several individual state-to-state processes (five transitions) exhibit cross sections different by a factor of 3 (for the two PESs). Only in this regime, the cross sections obtained from the present PES are systematically larger than those obtained from the PES of Vissers *et al.*[21] This is a minor difference that should have no effect on the results of modeling. Therefore, we conclude that the two PESs lead to very similar predictions of state-to-state transition cross sections and would result in similar rate coefficients and similar predictions of the overall kinetics for rotational–translational energy transfer between rigid CO molecules at intermediate and high collision energies. Still, small differences between the two PESs in the asymptotic range may affect the outcomes of CO + CO collisions at low energies, when the Coriolis coupling is more important.

Now we move to comparison of MQCT calculations for CO + CO against the full-quantum calculations of Żółtowski *et al.*,[19] carried out using MOLSCAT program and the PES of Vissers *et al.* To make the comparison straightforward, MQCT calculations presented below were carried out using the same PES of Vissers *et al.* These data are presented in Fig. 8 for 44 individual transitions that represent various excitations in the CO + CO system starting from its ground state $(j_1,j_2) = (0,0)$, at three collision energies. The agreement between the two methods is good overall, and is better at higher energies, as one may expect from the mixed quantum/classical nature of the MQCT method. Moreover, strong transitions with large cross sections are well reproduced by MQCT at all collision energies. This includes twelve transitions with total cross sections larger than 1 Å^2. For weaker transitions, with cross sections in the range from 0.1 to 1 Å^2, the results of MQCT are systematically smaller than the results of MOLSCAT. At higher energy (900 cm^{-1}) the differences are within a factor of 2 for most transitions, except

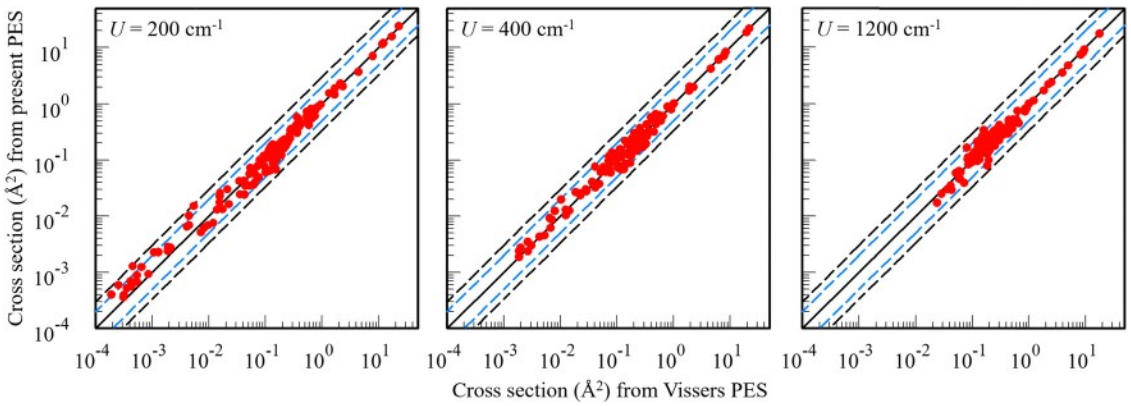

Fig. 7 Comparison of MQCT state-to-state transition cross sections for CO + CO system obtained using the present PES and Vissers *et al.* PES for three values of collision energy U (indicated in each frame). The initial state was (j_1,j_2) = (0,0). Blue dashed lines represent a factor of 2 difference and black dashed lines represent a factor of 3 difference.

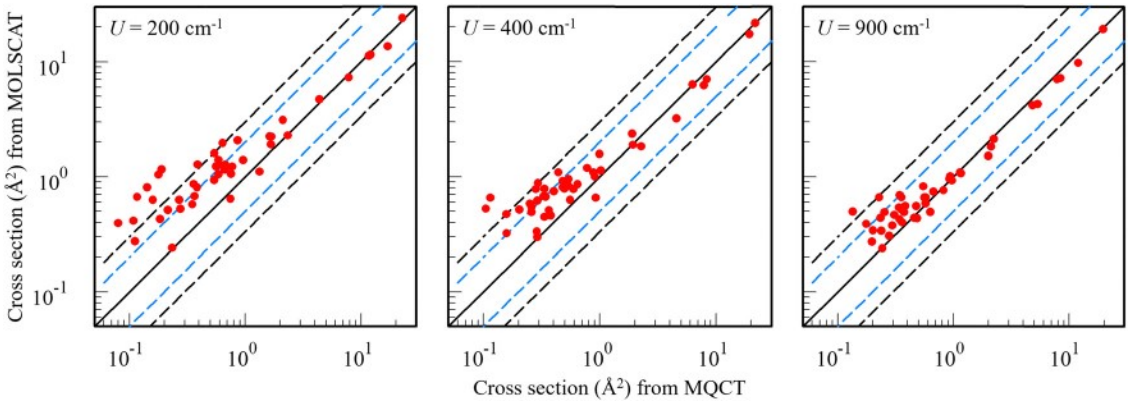

Fig. 8 Comparison of MQCT and MOLSCAT state-to-state transition cross sections for CO + CO system obtained using Vissers *et al.* PES. The initial state was (j_1,j_2) = (0,0); the final states are those reported in ref. 19 with all combinations of $j_1 \leq 8$ and $j_2 \leq 8$. Blue dashed lines represent a factor of 2 difference and black dashed lines represent a factor of 3 difference.

two very weak transitions where the difference is about a factor of 3. At 400 cm^{-1} the two weakest transitions deviate by more than a factor of 3, and at lower energy (200 cm^{-1}) the seven weakest transitions deviate by more than a factor of 3 (see Fig. 8). Again, larger errors at lower collision energy are expected for the trajectory based MQCT method.

In Fig. 9 we compare the dependencies of state-to-state transition cross sections on collision energy for the eleven most intense transitions that originate from the ground rotational state (j_1,j_2) = (0,0) of the CO + CO system, and for the elastic scattering channel (0,0) → (0,0). The final states are indicated in the individual frames of the figure and include up to four rotational quanta in each molecule, (j_1,j_2) = (4,4). Larger cross sections are presented closer to the upper left corner of the figure, while smaller cross sections are placed closer to the lower right corner of the figure. One can see that overall MQCT gives a consistently good picture of state-to-state transition processes in CO + CO system through a broad range of collision energies, except for the lowest energy range ~100 cm^{-1} and below, where the results of the full quantum calculations are dominated by scattering resonances. The excitations of states (j_1,j_2) = (0,1), (1,1), (1,2), (2,2), (0,3), (2,3) and (3,3) are reproduced particularly well, with differences between MQCT results and those of full-quantum calculations about 10%, on average. Larger relative differences are observed at low collision energies for excitations of (j_1,j_2) = (0,2), (2,4) and (4,4) states of CO + CO. Interestingly, the behavior of elastic scattering cross section (large values on the order of 200 $Å^2$) is also reproduced by MQCT reasonably well, on average, without high frequency oscillations.

At high collision energy the question of convergence of the full-quantum benchmark calculations of Żółtowski *et al.*[19] becomes important. Namely, in order to make those full-quantum calculations numerically affordable, the value of total angular momentum was restricted to $J_{TOT} \leq 190$ (see ref. 19) which corresponds to ℓ_{max} = 190 in MQCT calculations. Now recall that MQCT calculations reported here are done with the much larger value of ℓ_{max} = 345, because we found that ℓ_{max} = 190 is insufficient to obtain converged cross sections for four strong transitions: (0,0) → (0,1), (1,1), (0,2) and (2,2), see Fig. 4

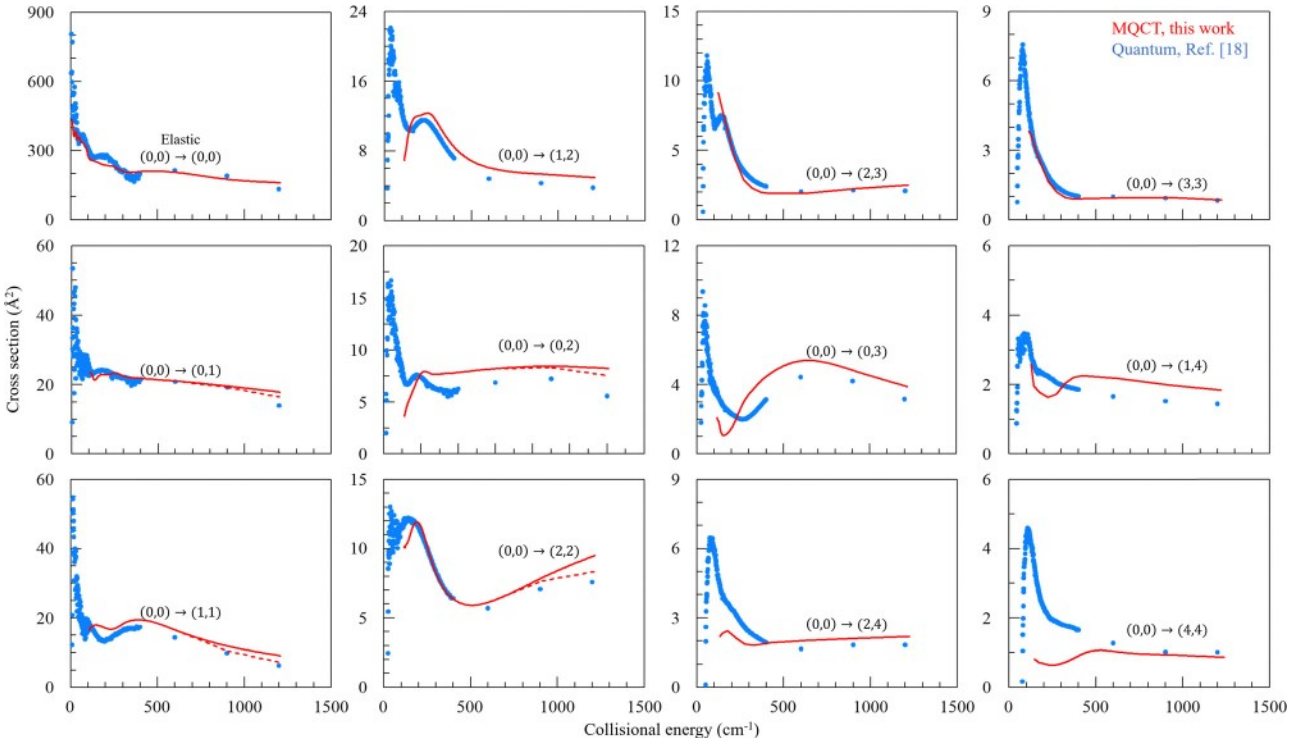

Fig. 9 Comparison of MQCT (red lines) and MOLSCAT (blue symbols) state-to-state transition cross sections for CO + CO system as a function of collision energy, obtained using Vissers *et al.* PES. The initial state was (j_1j_2) = (0,0); the final states are those 12 with largest cross sections, including the elastic channel (as indicated in each frame). Note that the vertical scales are different in different frames. Dashed lines are MQCT results obtained with ℓ_{max} reduced to 190, as in MOLSCAT calculations.

and its discussion above. Therefore, for a fair comparison of MQCT *vs.* full-quantum calculations, one should either increase the value of J_{TOT} in MOLSCAT up to 345, or decrease ℓ_{max} in MQCT calculations down to 190. Since the first option is computationally unfeasible, we carried out a numerical experiment in which we removed "by hand" all contributions of $\ell >$ 190 from MQCT cross sections. These data are presented in Fig. 9 by dashed lines. They indicate an improved agreement with full quantum results of Żółtowski *et al.*[19] at high energy, in particular for the excitation of state (2,2). This means that some of the differences seen in Fig. 9 are related to convergence of the quantum calculations, which in principle can be improved for an extra CPU cost.

Finally, we carried out MQCT calculations for the excitation and quenching of the excited rotational states (j_1j_2) = (0,8) and (8,8) for a collision energy 900 cm^{-1}. These data are presented in Fig. 10. They indicate the same level of agreement between MQCT and MOLSCAT as one presented in Fig. 8 above for the excitation of ground state (j_1j_2) = (0,0), which means that MQCT offers a consistent treatment of the various types of transitions that were explored in the CO + CO system.

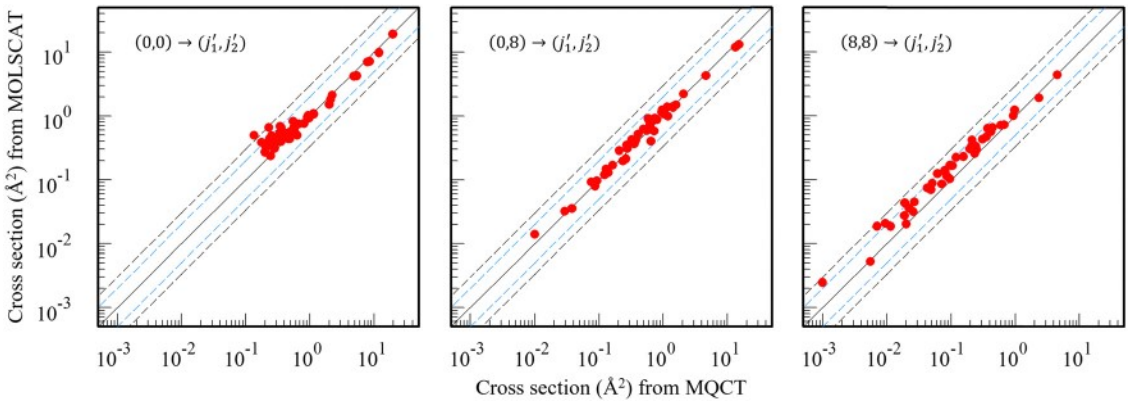

Fig. 10 The same figure as Fig. 8, for the total energy 900 cm^{-1} and three different initial states.

It is instructive to discuss the origin of differences between the results of MQCT and full-quantum calculations. Recall that both the full quantum calculations and the MQCT calculations presented in this paper were carried out within the coupled-states (CS) approximation that neglects the effect of Coriolis coupling. It is important to stress that, within this assumption, the state-to-state transition matrices are identical in the full-quantum approach and in MQCT. Therefore, the descriptions of the rotational motion of CO molecules, including their spectra of rotational states and the potential coupling between those states, are basically the same in the two methods. The differences come from the treatment of translational motion of two collision partners along the coordinate R that corresponds to the molecule–molecule distance. In the full quantum method this is done by wavefunctions described by a system of 2nd-order differential equations, propagated from $R = 0$ through interaction region into the asymptotic range, where the scattering matrix is computed. Step-size along R depends on the de Broglie wavelength and becomes very small if the collision partners are heavy (such as CO + CO) and/or when the collision energy is high (such as considered here). This property is a source of high numerical cost of the full-quantum calculations. In MQCT, in contrast, the motion along R is described classically using trajectories. Differential equations for time evolution of probability amplitudes are 1st-order, simpler to propagate, with step-size determined only by the interaction potential (independent of de Broglie wavelength and thus insensitive to masses or energy of collision partners) which makes MQCT affordable even for heavy collision partners and at high collision energy. Unfortunately, quantum effects associated with motion along R (such as scattering resonances at low collision energies) are missing. This explains the differences between MQCT and full-quantum calculations seen in Fig. 9, in particular at low collision energy, when quantum cross sections oscillate due to scattering resonances.

V. Conclusions

In this paper we present an updated version of the 2013 CO + CO potential energy surface of Dawes *et al.*[23] The new surface incorporates improved asymptotic behavior and for scattering purposes is somewhat different from another PES available for this system, that of Vissers *et al.*[21] This was confirmed quantitatively by expanding both surfaces over a set of analytic functions and comparing the behavior of expansion coefficients along the molecule–molecule distance R. We found that, although the behavior of all expansion coefficients is, overall, similar, there are some non-negligible differences in the attractive part of the PES, and some larger differences in the high energy region at small R, where the PES is repulsive. These differences have only a minor effect on strong state-to-state transitions with larger cross sections, but have a more sizable effect on weaker transitions, where the differences of cross sections up to a factor of two were observed for the two PESs. This was demonstrated by inelastic scattering calculations carried out using MQCT program[26,27] that implements the mixed quantum/classical theory for molecular energy exchange processes and permits to compute state-to-state transition cross sections at a much lower computational cost, compared to the full-quantum methods.

The validity of MQCT predictions of state-to-state transition cross sections was also assessed by comparison against the full-quantum results from ref. 18 and 19. MQCT calculations were carried out with a large basis set, a broad range of energies, a large range of collision impact parameters (large values of molecule–molecule orbital angular momentum quantum number up to $\ell \sim 335$), and for various initial states of CO + CO system. In all cases MQCT gives reliable results, except low collision energy (below around 100 cm^{-1}) where the full-quantum calculations predict strong oscillations of state-to-state transition cross sections. For strong dipole-driven transitions the results of MQCT are reliable, especially at higher collision energy. For weaker transitions and lower collision energies the cross sections predicted by MQCT may be a factor of 2–3 different from those obtained by full-quantum calculations for CO + CO. Although there was a significant recent interest in the experimental studies of CO rotational excitations,[22,49] there are no direct experimental measurements of absolute values of inelastic cross sections or rate coefficients for the rotational state-to-state transitions in CO + CO collisions, to the best of our knowledge. We hope that this theoretical work will stimulate new experimental efforts.

In this paper we presented the results obtained with two different dynamics methods (full-quantum and MQCT) combined with two different potential energy surfaces for rigid CO molecules (that of Vissers *et al.* and the present PES). In the future, these studies can be extended to include the vibrational motion of CO molecules using the PES of Chen *et al.* and employing the method of quasi-classical trajectories. This would represent a very comprehensive study of CO + CO system using three different dynamics methods combined with three different potential energy surfaces.

A new version of MQCT suite of codes[28] is always available to the community through GitHub.

Conflicts of interest

Authors declare no conflict of interests.

Acknowledgements

This research was supported by NSF grant number CHE-2102465. D. Babikov acknowledges the support of Way Klingler Research Fellowship and of the Haberman-Pfletschinger Research Fund. D. Bostan acknowledges the support of Eisch Fellowship and the Bournique Memorial Fellowship. CJ acknowledges the support of Schmitt Fellowship. R. D. and E. Q.-S. were supported by the U. S. Department of Energy (Award DE-SC0019740). A. B.-P. acknowledges the support of the MS&T's Kummer Institute through the Kummer Innovation

and Entrepreneurship Doctoral Fellowship. We used resources of the National Energy Research Scientific Computing Center, which is supported by the Office of Science of the U.S. Department of Energy under Contract No. DE-AC02-5CH11231. This research also used HPC resources at Marquette, funded in part by the National Science foundation award CNS-1828649. Martin Cordiner at NASA is acknowledged for stimulating discussions and his encouragement of this project.

References

1 A. L. Cochran, A.-C. Levasseur-Regourd, M. Cordiner, E. Hadamcik, J. Lasue, A. Gicquel, D. G. Schleicher, S. B. Charnley, M. J. Mumma and L. Paganini, *et al.*, The composition of comets, *Space Sci. Rev.*, 2015, **197**, 9–46.

2 C. Ceccarelli, P. Caselli, D. Bockelée-Morvan, O. Mousis, S. Pizzarello, F. Robert and D. Semenov, Deuterium fractionation: the Ariadne's thread from the pre-collapse phase to meteorites and comets today, *arXiv*, 2014, preprint, arXiv:1403.7143, DOI: 10.48550/arXiv.1403.7143.

3 S. Alan Stern, The evolution of comets in the Oort cloud and Kuiper belt, *Nature*, 2003, **424**, 639–642.

4 C. Opitom, A. Fitzsimmons, E. Jehin, Y. Moulane, O. Hainaut, K. J. Meech, B. Yang, C. Snodgrass, M. Micheli and J. V. Keane, *et al.*, 2I/Borisov: A C_2-depleted interstellar comet, *Astron. Astrophys.*, 2019, **631**, L8.

5 D. Jewitt, M.-T. Hui, Y. Kim, M. Mutchler, H. Weaver and J. Agarwal, The nucleus of interstellar comet 2I/Borisov, *Astrophys. J., Lett.*, 2020, **888**, L23.

6 A. Fitzsimmons, O. Hainaut, K. J. Meech, E. Jehin, Y. Moulane, C. Opitom, B. Yang, J. V. Keane, J. T. Kleyna and M. Micheli, *et al.*, Detection of CN gas in interstellar object 2I/Borisov, *Astrophys. J., Lett.*, 2019, **885**, L9.

7 P. Guzik, M. Drahus, K. Rusek, W. Waniak, G. Cannizzaro and I. Pastor-Marazuela, Initial characterization of interstellar comet 2I/Borisov, *Nat. Astron.*, 2020, **4**, 53–57.

8 M. A. Cordiner, S. N. Milam, N. Biver, D. Bockelée-Morvan, N. X. Roth, E. A. Bergin, E. Jehin, A. J. Remijan, S. B. Charnley and M. J. Mumma, *et al.*, Unusually high CO abundance of the first active interstellar comet, *Nat. Astron.*, 2020, **4**, 861–866.

9 D. Bodewits, J. W. Noonan, P. D. Feldman, M. T. Bannister, D. Farnocchia, W. M. Harris, J.-Y. Li, K. E. Mandt, J. W. Parker and Z.-X. Xing, The carbon monoxide-rich interstellar comet 2I/Borisov, *Nat. Astron.*, 2020, **4**, 867–871.

10 B. Yang, A. Li, M. A. Cordiner, C.-S. Chang, O. R. Hainaut, J. P. Williams, K. J. Meech, J. V. Keane and E. Villard, Compact pebbles and the evolution of volatiles in the interstellar comet 2I/Borisov, *Nat. Astron.*, 2021, **5**, 586–593.

11 D. Bodewits, B. P. Bonev, M. A. Cordiner and G. L. Villanueva, Radiative processes as diagnostics of cometary atmospheres, *arXiv*, 2022, preprint, arXiv:2209.02616, DOI: 10.48550/arXiv.2209.02616.

12 F. F. S. Van der Tak, J. H. Black, F. L. Schöier, D. J. Jansen and E. F. van Dishoeck, A computer program for fast non-LTE analysis of interstellar line spectra-With diagnostic plots to interpret observed line intensity ratios, *Astron. Astrophys.*, 2007, **468**, 627–635.

13 C. Brinch and M. R. Hogerheijde, LIME–a flexible, non-LTE line excitation and radiation transfer method for millimeter and far-infrared wavelengths, *Astron. Astrophys.*, 2010, **523**, A25.

14 A. Faure, F. Lique and J. Loreau, The effect of CO–H_2O collisions in the rotational excitation of cometary CO, *Mon. Not. R. Astron. Soc.*, 2020, **493**, 776–782.

15 M.-L. Dubernet and E. Quintas-Sánchez, First quantum study of the rotational excitation of HCN by para-H_2O: Convergence of quantum results, influence of the potential energy surface, and approximate rate coefficients of interest for cometary atmospheres, *Mol. Astrophys.*, 2019, **16**, 100046.

16 C. Boursier, B. Mandal, D. Babikov and M. L. Dubernet, New H_2O–H_2O collisional rate coefficients for cometary applications, *Mon. Not. R. Astron. Soc.*, 2020, **498**, 5489–5497.

17 B. Mandal and D. Babikov, Rate coefficients for rotational state-to-state transitions in H_2O + H_2O collisions for cometary and planetary applications, as predicted by mixed quantum-classical theory, *Astron. Astrophys.*, 2023, **671**, A51.

18 M. Żółtowski, J. Loreau and F. Lique, Collisional energy transfer in the CO–CO system, *Phys. Chem. Chem. Phys.*, 2022, **24**, 11910–11918.

19 M. Żółtowski, F. Lique, J. Loreau, A. Faure and M. Cordiner, The excitation of CO in CO-dominated cometary comae, *Mon. Not. R. Astron. Soc.*, 2023, **520**, 3887–3894.

20 S. A. Ndengué, R. Dawes and F. Gatti, Rotational Excitations in CO-CO Collisions at Low Temperature: Time-Independent and Multiconfigurational Time-Dependent Hartree Calculations, *J. Phys. Chem. A*, 2015, **119**, 7712–7723.

21 G. W. M. Vissers, P. E. S. Wormer and A. Van Der Avoird, An *ab initio* CO dimer interaction potential and the computation of the rovibrational spectrum of $(CO)_2$, *Phys. Chem. Chem. Phys.*, 2003, **5**, 4767–4771.

22 Z.-F. Sun, M. C. van Hemert, J. Loreau, A. van der Avoird, A. G. Suits and D. H. Parker, Molecular square dancing in CO–CO collisions, *Science*, 1979, **2020**(369), 307–309.

23 R. Dawes, X. G. Wang and T. Carrington, CO dimer: New potential energy surface and rovibrational calculations, *J. Phys. Chem. A*, 2013, **117**, 7612–7630.

24 J. Chen, J. Li, J. M. Bowman and H. Guo, Energy transfer between vibrationally excited carbon monoxide based on a highly accurate six-dimensional potential energy surface, *J. Chem. Phys.*, 2020, **153**, 54310.

25 W. Bohn, H. Von Bülow, S. Dass, A. A. Ionin, Y. M. Klimachev, A. A. Kotkov, J. K. McIver, J. E. McCord, L. V. Seleznev and D. V. Sinitsyn, *et al.*, High-power supersonic CO laser on fundamental and overtone transitions, *Quantum Electron.*, 2005, **35**, 1126.

26 A. Semenov, B. Mandal and D. Babikov, MQCT: User-ready program for calculations of inelastic scattering of two molecules, *Comput. Phys. Commun.*, 2020, **252**, 107155.

27 B. Mandal, C. Joy, D. Bostan, A. Eng and D. Babikov, Adiabatic Trajectory Approximation: A New General Method

in the Toolbox of Mixed Quantum/Classical Theory for Collisional Energy Transfer, *J. Phys. Chem. Lett.*, 2023, **14**, 817–824.
28 B. Mandal, D. Bostan, C. Joy and D. Babikov, MQCT 2024: A program for calculations of inelastic scattering of two molecules (new version announcement), *Comput. Phys. Commun.*, 2024, **294**, 108938.
29 G. D. Billing, *The quantum classical theory*, Oxford University Press, 2003.
30 A. Semenov, M. Ivanov and D. Babikov, Ro-vibrational quenching of CO (v = 1) by He impact in a broad range of temperatures: A benchmark study using mixed quantum/classical inelastic scattering theory, *J. Chem. Phys.*, 2013, **139**, 74306.
31 D. Babikov and A. Semenov, Recent advances in development and applications of the mixed quantum/classical theory for inelastic scattering, *J. Phys. Chem. A*, 2016, **120**, 319–331.
32 E. Castro-Juárez, X.-G. Wang, T. Carrington Jr, E. Quintas-Sánchez and R. Dawes, Computational study of the ro-vibrational spectrum of CO–CO_2, *J. Chem. Phys.*, 2019, **151**, 84307.
33 E. Quintas-Sánchez, R. Dawes, X.-G. Wang and T. Carrington, Computational study of the rovibrational spectrum of CO_2–N_2, *Phys. Chem. Chem. Phys.*, 2020, **22**, 22674–22683.
34 B. Desrousseaux, E. Quintas-Sánchez, R. Dawes, S. Marinakis and F. Lique, Collisional excitation of interstellar PN by H_2: New interaction potential and scattering calculations, *J. Chem. Phys.*, 2021, **154**, 34304.
35 M. Gancewski, H. Jóźwiak, E. Quintas-Sánchez, R. Dawes, F. Thibault and P. Wcisło, Fully quantum calculations of O_2–N_2 scattering using a new potential energy surface: Collisional perturbations of the oxygen 118 GHz fine structure line, *J. Chem. Phys.*, 2021, **155**, 124307.
36 A. Zadrożny, H. Jóźwiak, E. Quintas-Sánchez, R. Dawes and P. Wcisło, *Ab initio* quantum scattering calculations for the CO–O_2 system and a new CO–O_2 potential energy surface: O_2 and air broadening of the R (0) line in CO, *J. Chem. Phys.*, 2022, **157**, 174310.
37 A. Olejnik, H. Jóźwiak, M. Gancewski, E. Quintas-Sánchez, R. Dawes and P. Wcisło, *Ab initio* quantum scattering calculations and a new potential energy surface for the HCl ($X_1\Sigma^+$)–O_2 ($X_3\Sigma_g^-$) system: Collision-induced line shape parameters for O_2-perturbed R (0) 0–0 line in $H^{35}Cl$, *J. Chem. Phys.*, 2023, **159**, 134301.
38 E. Quintas-Sánchez and R. Dawes, AUTOSURF: A Freely Available Program To Construct Potential Energy Surfaces, *J. Chem. Inf. Model.*, 2019, **59**, 262–271.
39 R. Dawes and E. Quintas-Sánchez, *Reviews in Computational Chemistry* vol. 31, 2018, pp. 199–264.
40 M. Majumder, S. A. Ndengué and R. Dawes, Automated construction of potential energy surfaces, *Mol. Phys.*, 2016, **114**, 1–18.
41 R. Dawes, X.-G. Wang, A. W. Jasper and T. Carrington Jr, Nitrous oxide dimer: A new potential energy surface and rovibrational spectrum of the nonpolar isomer, *J. Chem. Phys.*, 2010, **133**, 134304.
42 H.-J. Werner, P. J. Knowles, G. Knizia, F. R. Manby and M. Schütz, Molpro: a general-purpose quantum chemistry program package, *Wiley Interdiscip. Rev.: Comput. Mol. Sci.*, 2012, **2**, 242–253.
43 G. Knizia, T. B. Adler and H.-J. Werner, Simplified CCSD(T)-F12 methods: Theory and benchmarks, *J. Chem. Phys.*, 2009, **130**, 54104.
44 D. W. Schwenke, The extrapolation of one-electron basis sets in electronic structure calculations: How it should work and how it can be made to work, *J. Chem. Phys.*, 2005, **122**, 014107.
45 I. M. Sobol, Uniformly distributed sequences with an additional uniform property, *USSR Comput. Math. and Math. Phys.*, 1976, **16**, 236–242.
46 A. Semenov and D. Babikov, Mixed quantum/classical calculations of total and differential elastic and rotationally inelastic scattering cross sections for light and heavy reduced masses in a broad range of collision energies, *J. Chem. Phys.*, 2014, **140**, 44306.
47 A. Semenov and D. Babikov, Inelastic Scattering of Identical Molecules within Framework of the Mixed Quantum/Classical Theory: Application to Rotational Excitations in H_2 + H_2, *J. Phys. Chem. A*, 2016, **120**, 3861–3866.
48 A. Semenov and D. Babikov, Mixed quantum/classical theory for molecule–molecule inelastic scattering: derivations of equations and application to N_2+ H_2 system, *J. Phys. Chem. A*, 2015, **119**, 12329–12338.
49 M. R. Laskowski, T. J. Michael, H. M. Ogden, M. H. Alexander and A. S. Mullin, Rotational energy transfer kinetics of optically centrifuged CO molecules investigated through transient IR spectroscopy and master equation simulations, *Faraday Discuss.*, 2022, **238**, 87–102.